Eocene to Oligocene Cooling and Ice Growth based on the Geochemistry of Interglacial Mudstones from the East Antarctic Continental Shelf

Jennifer J. Light and Sandra Passchier[1]

Department of Earth and Environmental Studies, Center for Environmental and Life Sciences
Montclair State University, 1 Normal Ave, Montclair N.J. 07043, U.S.A.

[1]Corresponding author: passchiers@montclair.edu ORCID: 0000-0001-7204-7025

Abstract

The Eocene Oligocene Transition at ~34 million years ago (Ma), marked the global change from greenhouse to icehouse, and the establishment of the East Antarctic Ice Sheet (EAIS). How the ice-sheet behavior changed during interglacials across this climate transition is poorly understood. We analyzed major, trace and rare earth elemental (REE) data of late Eocene interglacial mudstone from Prydz Bay at ODP Site 1166 and early Oligocene interglacial mudstone from IODP Site U1360 on the Wilkes Land continental shelf. Both sites have comparable glaciomarine depositional settings. Lithofacies and provenance at Site 1166 in Prydz Bay is indicative of a late Eocene glacial retreat in the Lambert Graben. Paleoclimate proxies, including the Chemical Index of Alteration (CIA), mean annual temperature (S-index), and mean annual precipitation (CIA-K) show a dominant warm humid paleoclimate for the late Eocene interglacial. In contrast, at Site U1360, in the early Oligocene, provenance and interglacial weathering regime remained relatively stable with conditions of physical weathering. These results confirm that the EAIS substantially retreated periodically during late Eocene interglacials, and that subglacial basins likely remained partially glaciated during interglacials in the earliest Oligocene.

Key Words: geochemistry, sediment, glaciation, REE

Introduction

Due to ice coverage, what is currently known about the geology of the Antarctic continent comes from sparse outcrops and proxy data from marine sediment cores. Antarctica was not always ice covered; paleo-reconstructions show that the continental conditions were much warmer and with reduced ice extent during the Eocene Epoch (Pross *et al.*, 2012). The Eocene Epoch (~56 – 34 Ma) marked a time of great change in global climate from the Early Eocene Climatic Optimum (Zachos *et al.*, 2001; Westerhold *et al.*, 2020), to the arrival of polar glaciation in the late Eocene and into the Oligocene. The transition from Eocene greenhouse conditions to Oligocene cooling conditions is documented by a distinct increase in benthic foraminifera $\delta^{18}O$ values (Zachos *et al.*, 2001; Coxall *et al.*, 2005). The changes are documented as two distinct steps, the EOT-1 (34.4 Ma), and the Oi-1 (Oligocene isotope event-1, 33.7 Ma); the first is attributed to cooling and the later to significant ice growth of the East Antarctic Ice Sheet (EAIS) (Coxall *et al.*, 2005).

The Eocene Oligocene Transition has been widely modeled to better understand the initiation, and intensification of glaciation in Antarctica (Wilson *et al.*, 2013; Ladant *et al.*, 2014; Van Breedam *et al.*, 2022). DeConto *et al.* (2003) posited that the onset of glaciation was likely due to a decrease in atmospheric CO_2, which could have caused the initial cooling necessary for ice caps to begin growing. The opening of the Tasman and Drake passages and subsequent isolation of the Antarctic continent along with the Miocene formation of the Antarctic Circum-polar Current (ACC) would have been a secondary mechanism for cooling (DeConto *et al.*, 2003, Gasson *et al.*, 2014, Goldner *et al.*, 2014), potentially allowing for ice sheet growth. These models suggests that under these conditions the growth of the EAIS would have nucleated in areas of high topographic relief and expanded outward toward the coasts, reaching the marine environment first in the Dronning Maud Land, then Prydz Bay and finally the Wilkes Land/Terra Adélie coast (DeConto *et al.*, 2003; Stocchi *et al.*, 2013). Gasson *et al.* (2014) and Van Breedam *et al.* (2022) highlight the sensitivity of EAIS growth in ice-sheet models to paleotopographical boundary conditions. However, even under the maximum paleotopography reconstructed by Wilson *et al.* (2014) and Paxman *et al.* (2019), the ice sheet model by Van Breedam *et al.* (2022) still produces significant ice sheet reduction during late Eocene interglacials due to the sensitivity of the ice sheet to relatively small changes in CO_2 around a threshold value.

Two sites on the East Antarctic margin contain mudstones that allow us to investigate the paleoclimate conditions through Eocene and Oligocene interglacials. Updated detailed age models show that ODP Site 1166 and IODP Site U1360 contain upper Eocene and lower Oligocene sediments respectively (Florindo *et al.*, 2003; Houben *et al.*, 2013; Passchier *et al.*, 2017). Despite the limited thickness and recovery of sediments, the sites were chosen because they include the most complete Eocene and Oligocene deglacial sequences on the East Antarctic continental shelf that were deposited during interglacials. The fine-grained lithologies allow for the application of a detrital geochemical approach, including the application of inorganic paleoclimate proxies, such as the Chemical Index of Alteration and the S-index (Nesbitt & Young, 1981; Sheldon *et al.*, 2002). By reconstructing the mud provenance and weathering indices of the interglacial sediments, the changing paleoclimate of ice-sheet minima through the Eocene Oligocene Transition can be better understood.

Regional geology and previous work

Site 1166 is located in Prydz Bay, the main drainage basin for the Lambert Glacier-Amery Ice Shelf that today drains ~20% of the of the EAIS (van de Flierdt *et al.*, 2008). The Amery Ice Shelf and Prydz Bay are located in the Lambert Graben, a failed arm of a triple junction, formed during the late Paleozoic to early Mesozoic as India began to rift from Antarctica (Stagg, 1985; Lisker *et al.*, 2003; Thomson *et al.*, 2013). On the Western edge of the Graben are the Northern and Southern Prince Charles Mountains, containing outcrops of Archean mafic dykes (Mikhalsky *et al.*, 2013), Precambrian granitic basement, metasedimentary rocks, high-grade metamorphic rocks, granitoids and volcanics, Cambrian granites, and Permian sedimentary rocks (Sheraton *et al.*, 1996; Munksgaard *et al.*, 1992). To the East of the Lambert Graben are the Grove Mountains that consist of Precambrian felsic orthogneisses, mafic granulites, and paragneiss (Figure 1) (Liu *et al.*, 2007). Located South of the Prince Charles Mountains and inland from the Lambert Graben are the Gamburtsev Subglacial Mountains. These mountains are ~3000 m in elevation and reside in the middle of the East Antarctic craton; they are believed to be an important nucleation point for Eocene Oligocene Transition ice growth (van de Flierdt *et al.*, 2008; DeConto & Pollard, 2003). The rock types of the Gamburtsev Subglacial Mountains remain unknown due to thick ice cover; however, recent studies suggest that they may be composed of mafic granitoids that have two age ranges, 650-500 Ma and 1100-800 Ma (Veevers *et al.*, 2008).

Sediment transport to Site 1166 in the late Eocene was dominantly glacio-fluvial; glacial textures on quartz grains were found in Unit II, indicating a proglacial environment (Strand *et al.*, 2003). Macphail and Truswell (2004) determined based on terrestrial palynology from Site 1166 that during the Eocene the region contained rainforest scrub lands indicating warm and wet environments. Thermochronological data from sample 16R-55cm in the section studied here (Figure 2) and the underlying Eocene sands indicate that erosion rates were low, and a very narrow detrital Apatite Fission Track (APT) age range of 250-300 Myr points to sediment transport confined to the Lambert Graben with limited erosion of Cretaceous ultramafic rocks exposed in MacRobertson Land (Thomson *et al.*, 2013). Through Nd-isotope studies, van de Flierdt *et al.*, (2008) had already suggested a Proterozoic to Cambrian age of source rocks within the Lambert Graben and the Gamburtsev Mountains for the Eocene mudstones from Site 1166. Epsilon-Nd ratios suggest that the upper part of Unit II at Site 1166 was likely sourced from an older potentially Archean/Paleoproterozoic parent material. The geochemical signature of the bulk sediment will be used here to better understand the provenance evolution of the sediments from Unit II, and its implications for ice advance and retreat within the Lambert Graben.

Site U1360 is found off the George V coast of the Wilkes Land province. During the late Cretaceous this region underwent rifting from Australia creating the continental margin. As spreading continued through the Eocene an open marine environment formed (Expedition 318 Scientists, 2010). Today, the shelf in this region is fed by sediments transported from the Wilkes Subglacial Basin. Outcrops and erratics show that inland, the bedrock geology of the region is dominated by Late Archean and Early Proterozoic paragneisses and granitoids, Early Proterozoic metasedimentary rocks, Early to Mid-Proterozoic granitoids and migmatites, Cambrian granites, Triassic sandstones, and Jurassic dolerites (Goodge & Fanning, 2010; Williams *et al.*, 2017; Godard *et al.*; 2019), and rhyolites from further inland (Peucat *et al.*, 2002). Understanding of the subglacial geology is further enhanced through correlation between Australian geological evidence and geophysical data. Aeromagnetic interpretations suggest the Wilkes Subglacial Basin consists of a low-lying metasedimentary basement incised with three extensional basins (Ferracioli *et al.*, 2009; Jordan *et al.*, 2013; Aitken *et al.*, 2014). The Wilkes Basin is bounded to the west by the Mertz Shear Zone and the Mawson Craton and to the east by a possible magmatic arc terrane (Ferracioli *et al.*, 2009; Jordan *et al.*, 2013; Aitken *et al.*, 2014). Towards the Transantarctic Mountains, the basement is interpreted to be covered by Jurassic Ferrar Dolerite (Jordan *et al.*, 2013) (Figure 1). The depositional environment for the lower Oligocene interglacial mudstones recovered at Site U1360 can be interpreted as glaciomarine with sea ice based on the presence of gravel-sized outsized clasts interpreted as ice-rafted debris and dinocyst assemblages (Houben *et al.*, 2013; Passchier *et al.*, 2019).

Methods and materials

Study sites

Ocean Drilling Program (ODP) Hole 1166A was drilled in Prydz Bay during ODP expedition 188 in 475.4 m of water depth, and down to 381.3 mbsf (Shipboard Scientific Party, 2001). This hole was divided into units based on lithology. This study will utilise samples from what has been classified as Unit II consisting of mudstones with dispersed clasts with interbeds of sand between 135.63 and 156.62 mbsf (Figure 2)(Shipboard Scientific Party, 2001). Hole U1360A was drilled by the Integrated Ocean Drilling Program (IODP) on Expedition 318 at 66°22.0395′S and 142°44.7050′E off the Terre Adélie Coast in 495 m of water depth. The hole was drilled to 70.8 msbf (Expedition 318 Scientists, 2010). The percentage of recovered material was 10%. For this study, we will be focusing on samples from Unit II specifically cores 3R through 6R (Figure 3). Investigations of the bulk detrital provenance and weathering history of sediments are ideally carried out on mudstones to avoid grain-size effects (Nesbitt & Young, 1981; McLennan, 2001; Von Einatten *et al.*, 2012). Particle size data from Sites 1166 and U1360 (Passchier *et al.*, 2017; 2019) indicate that the majority of samples from the two sites comprise <40% sand, > 60% silt, and <20% clay with a few exceptions (Figure 4).

Age Model

Detailed magnetobiostratigraphic age models have been developed for Sites 1166 (Shipboard Scientific Party, 2001), and Site U1360 (Expedition 318 Scientists, 2010). Originally, Hole 1166A was thought to contain late Eocene to early Oligocene sediment in what was classified as lithostratigraphic Unit II (Shipboard Scientific Party, 2001). However, Florindo *et al.* (2003) conducted a paleomagnetic study, creating an updated age model for Site 1166 by constraining paleomagnetic data with diatom and radiolarian assemblages. Based on the paleomagnetic data and diatom assemblages, it was interpreted that Unit II could have coincided with Chron 12r and Chron 13n, or Chron 15r through Chron 17 (Florindo *et al.*, 2003). Using the first occurrence of the dinoflagellate *Deflandrea* sp. A., Passchier *et al.* (2017) placed Unit II in the latter category, correlating the lower part of Unit II to Chron 16n.1n. The reversal located in the upper section of Unit II would then be Chron 15r, indicating that Unit II is late Eocene in age (Passchier *et al.*, 2017). Based on the magnetobiostratigraphic interpretation, the sandy mudstones in Unit II are dated to the interglacial between ~35.8 and 35.7 Ma, calibrated to the Vandenberghe *et al.*, (2012) time scale (Figure 5).

Initial ages for Unit II of Site U1360 were dated as early Oligocene based on diatoms and dinocysts (Expedition 318 Scientists, 2010). Reversed polarity was found in two samples from Site U1360 that correlated to Chron 12r, in combination with the biostratigraphy it provided a reliable Oligocene age (Expedition 318 Scientists, 2010). Houben *et al.* (2013) published an updated magnetobiostratigraphic age model for Site U1360. The updated age model was based on the first occurrence of the fossil taxa *Malvinia escutiana* that coincides with the Oi-1 oxygen isotope excursion event (Houben *et al.*, 2013). *Malvinia escutiana* first occurs at 42.02 mbsf in core 5R, and from 5R to 3R Oligocene diatom taxa, such as *Goniothecium rogersii*, *Hemiaulus* sp., *Pyxilla* sp., *Stephanopyxis* sp., *Fragilaria* spp., and *Kisseleviella cicatricata* were found (Houben *et al.*, 2013). Magnetic polarity showed a normal interval in Core 6R and a reversed polarity interval in cores 4R and 3R; based on the taxa and polarity intervals, it was determined that core 6R likely matched Chron 13n, which would suggest that the reversal located above, was dated to the base of Chron 12r (Houben *et al.*, 2013). The sedimentary facies succession that was recovered, the total thickness and sedimentation rates are consistent with a typical deglacial sequence on the East Antarctica continental margin (cf. Passchier *et al.*, 2019). Therefore, we interpret the mudstone sequence as sampling the earliest Oligocene deglaciation ~33.1 Ma (Figure 5).

Geochemical analysis

Preparation and analysis of samples was based on the shipboard guidelines of Murray *et al.* (2000) and analysis was carried out on a Horiba Jobin-Yvon Ultima inductively coupled plasma-optical emission spectrometer (ICP-OES) and Thermo Scientific iCap Q inductively coupled plasma-mass spectrometer (ICP-MS) at Montclair State University. Major, trace, and REE intensities were used to calculate paleoclimate proxies, changes in provenance, and elemental enrichments for Sites 1166 and U1360.

ICP-OES was conducted on 27 samples from Site 1166 and 9 samples from Site U1360. Samples were first powdered using an alumina mortar and pestle. Powdered samples were then weighed to 100 mg and dry mixed with 400 mg of lithium metaborate. Blanks of lithium metaborate alone were also weighed, and the sample mixtures, along with the blanks, were placed in graphite crucibles and heated in a furnace to 1050˚C for 30 minutes. Crucibles were removed from the furnace, swirled, and replaced for an additional 10 minutes. Crucibles were then removed from the furnace, and the samples were digested in 50 mL of 7% nitric acid, and filtered into 60 mL Nalgene sample bottles to acquire a concentration of 500x sample solution. From the 500x solution, a 4,000x solution was created for the sample analysis on the OES, by pipetting 6.5 mL of 500x solution into a bottle and adding 50 mL of 2% nitric acid. Both the 500x solution and the 4,000x solution sample bottles were stored in a refrigerator to reduce the chance of chemical reactions occurring in the samples. Subsequently, the 4,000x solutions were poured into test tubes and placed in an organized rack formation for analysis. Ten calibration standards from the United States Geological Survey (USGS) (i.e., DNC-1, BHVO2, W2, BCR2, AGV2, GSP2, BIR, G2, QLO1, and RGM-1) and two internal standards (MAG-1, SCO1) were also prepared in the same manner and added to the rack for analysis. Samples for ICP-MS analysis were diluted to a 10,000x solution from the original 500x solution used for ICP-OES analysis. The 10,000x solution was prepared by pipetting .5 mL of 500x solution into a test tube and diluting it with 9.5 mL of 2% nitric acid.

Provenance tracing

Aluminum and titanium are conservative elements, meaning they are not easily altered in the surface environment or the water column during sedimentation and carry the signature of their source rock. This allows the wt.% ratio of Al_2O_3/TiO_2 to show changes in source rock over time throughout the core. To better constrain provenance at Sites 1166 and U1360, trace and REE elements were used to create bivariate ratio plots. Enrichments of Rare Earth Elements (REE) were calculated using the normalized wt.% and normalized ppm of elements in each sample divided by the Post-Archean Average Australian Shale (Taylor & McLennan, 1985; Barth *et al.*, 2000). Values were then set to a logarithmic scale; values above 1 indicate enrichment, while values below 1 indicate a depletion of that element in the sample.

Weathering proxies

The Chemical Index of Alteration (Nesbitt and Young, 1982) is used on mud-rocks to calculate the degree of chemical weathering from the molar concentrations of Al_2O_3, CaO, Na_2O and K_2O, using equation (2).

$$CIA = \left[\frac{Al_2O_3}{Al_2O_3 + CaO + Na_2O + K_2O}\right] * 100 \tag{2}$$

CIA values greater than 65 indicate an environment prone to chemical weathering likely warmer and more humid, whereas values below 65 indicate an environment prone to physical weathering and an increase in glacial rock flour (Nesbitt & Young, 1982; Passchier *et al.*, 2017), likely an indication of glacial growth.

The molar value of CaO in the CIA calculation needs to be the silicate mineral contribution of CaO. Bulk samples may contain calcium in the form of calcium carbonate ($CaCO_3$) and a carbonate correction is typically carried out. However, upon exposure to 10% HCl splits of the mud samples showed a very weak reaction or no reaction at all. Furthermore, measured CaO values in the samples were very low. Therefore, a carbonate correction was not used for either site 1166 or U1360 in calculating the CIA values.

MAP and MAT were calculated using mudrocks from Sites 1166 and U1360 according to methods from Passchier *et al.* (2013) and Sheldon *et al.* (2002). MAP for each site was calculated using equation (3).

$$MAP = 143.75e^{0.0232(CIA-K)} \tag{3}$$

To calculate MAP, the equation requires a version of the CIA in which K_2O is removed, known as the CIA-K (Passchier *et al.*, 2013, Sheldon *et al.*, 2002).

MAT was calculated using equation four, in which S is the molar ratio of K_2O and Na_2O to Al_2O_3 (Sheldon *et al.*, 2002).

$$MAT = -18.5(S) + 17.3 \tag{4}$$

Once values were calculated for both MAP and MAT they were compared to previously published precipitation and temperature data (Passchier *et al.*, 2013; Macphail & Truswell, 2004; Tibbett *et al.*, 2021), based on both terrestrial climofunctions and palynology.

Results

Mud provenance

The first step in provenance tracing was to calculate elemental ratios that track detrital minerals at each site to determine if there were changes in the values, that would indicate a change in source material. To check for grain size effects on the data, bubble plots were created where the size of the marker is equivalent to the sand % in the < 2mm fraction (Figure 6). High field strength elements Zr, Hf, Nb, Ta and Al and Ti are typically partitioned in the detrital fraction of marine sediments and can be used as provenance tracers (e.g., Bonjour and Dabard, 1991; Plank & Langmuir, 1998; Young & Nesbitt, 1998). Zr/Hf ratios in pelagic marine sediments are typically ~35 (Plank & Langmuir, 1998), and for the PAAS ~42 (McLennan, 2001), whereas Nb/Ta for both are ~14. In comparison, the Zr/Hf ratios for the Antarctic mudstones fall between 35 and 42 and mudstones also show a larger range of values for Nb/Ta, between 9 and 18, suggestive of variable local source rock compositions directly upstream (Foley *et al.*, 2002). The Al_2O_3/TiO_2 values at Site 1166 ranged from ~18 to 25, which is not a large range, suggesting mostly mafic to intermediate rocks in the source areas. In contrast, Al_2O_3/TiO_2 of Site U1360 sediments revealed values ranging from ~21 to ~46, and this large range suggests that the sediments were sourced from different intermediate and felsic types of source rocks through time.

A Th/Sc versus Zr/Sc plot was produced to determine if the samples showed effects of sediment recycling and sorting (McLennan *et al.*, 1993). Th/Sc values are generally higher for mudstones from Site 1166 in Prydz Bay than for mudstones from Site U1360. For both locations Zr/Sc slightly increase with grain-size (Figure 6C)(McLennan *et al.*, 1993); La/Th and Hf values are very similar to PAAS (Figure 6D). Cr/V ratios for Site 1166 are slightly elevated over PAAS, and Y/Ni ratios are elevated for the majority of samples and more spread-out for Site 1166 (Figure 6E).

Elemental spider diagrams were created for REE elements normalized to the PAAS (Figure 7). Sediments from Site U1360 are similar in REE distribution to PAAS, although some samples (those from core 6R) are depleted in LREE. In contrast, sediments from Site 1166 in Prydz Bay show elevated REE abundances relative to PAAS, especially for the LREE. The Eu-anomaly and chrondrite normalized Gd/Yb ratios of the 1166 and U1360 sediments are similar to those of average post-Archean sedimentary rocks (Supplemental Figure 2).

Chemical Index of Alteration

Site 1166, Unit II, shows CIA values for the upper Eocene to be between 68 and 81 (Figure 2). The overlying Neogene glacial diamict shows a value of 57. Shipboard logs for Site 1166 show carbonate values up to 3.340% in some core intervals (O'Brien *et al.*, 2001). However, in the mudstone samples selected for this study at Site 1166 CaO were so low that even applying a small correction generated negative CaO values. For Site U1360, the shipboard data documented carbonate values up to 0.683%. To check for the impact of small amounts of carbonate on the CIA a carbonate correction was simulated for Site U1360 data at 0% and 1% $CaCO_3$. CIA values calculated at 0% carbonate range from 56-59, while CIA values calculated with a 1% carbonate correction range from 58-61 for the early Oligocene (Figure 3). At Site 1166, upper Eocene values are greater than 65 and are consistent with a chemical weathering regime (Nesbitt & Young, 1982). In contrast, lower Oligocene sediments from Site U1360 contain values less than 65, consistent with a dominant physical weathering regime.

Mean Annual Precipitation/Mean Annual Temperature

Calculated MAP for the upper Eocene mudstones in Prydz Bay showed values between ~906 mm to ~1171 mm (Figure 2). For Site U1360, applying a simulated carbonate correction of 1%, values with no carbonate correction range from 631 mm to 731 mm, while values that were carbonate corrected ranged from 674 mm to 817 mm (Figure 3). The 1% change in carbonate accounts for a difference of between 43 mm and 91 mm annually. Calculated MAT in the Prydz Bay upper Eocene mudstones fluctuate between 10.2°C and 13.7°C (Figure 2). The trend plots similarly to CIA values, showing a drop of ~2°C from 156.26 to 153.81 mbsf, and fluctuations between 10°C and 11.5°C up-core. There is a marked upward increase to 13.7°C at ~138 mbsf, consistent with peaks in CIA values and precipitation. In comparison to the upper Eocene mudstones from Site 1166 the lower Oligocene mudstones from Site U1360 show lower temperatures ranging from 8.2°C to 10.4°C (Figure 3). The trend in temperature appears to show a ~2°C warming up core and later a similar amount of cooling (Figure 3). Standard errors were calculated for both MAP and MAT proxies by Sheldon *et al.*, (2002) and show values of +/- 182 mm and +/- 4.4˚C, respectively.

Discussion

Site 1166

Initial analysis of the elements downcore showed an upward increase in mafic elements Cr, Ni, and V and an increase in Cr/V ratio (Figure 6). A particle size influence was ruled out, but higher CIA values in core 15R (Figure 2) correlate to the elevated ppm in Cr and Ni, which can be enriched in sediment due to the chemical weathering of olivine and orthopyroxene derived from ultramafic source rocks (Malkovski *et al.*, 2019). Furthermore, the upper Eocene mudstones are enriched in REE compared to PAAS (Figure 7). Such an enrichment is explained by a larger component of heavy minerals in the Prydz Bay sediment due to erosion of (ultra)mafic crystalline basement rocks (see also Supplemental Figure 1).

The Northern Prince Charles Mountains and the Grove Mountains, both contain mafic granulites (Munksgaard *et al.*, 1991; Liu *et al.*, 2007), and the Southern Prince Charles Mountains contain a swarm of mafic dykes (Mikhalsky *et al.*, 2013). However, the Northern and Southern Prince Charles Mountains include sequences of sedimentary or metasedimentary rocks, which typically dilute the heavy mineral component as a source; this is incompatible with the REE enrichment (Figure 7). Moreover, the Northern Prince Charles Mountains host Cretaceous intrusions, and according to apatite fission track ages obtained from Unit II at Site 1166, the coarse sediment fraction in this unit does not contain material of Cretaceous age (Thomson *et al.*, 2013). This makes a reasonable case for either the Grove Mountains or the Gamburtsev Subglacial Mountains as possible sources for the mafic material. Spatial distributions of elemental ratios of Nb/Ta, Sm/Zr, Cr/V and Al/Ti in basement rocks around Prydz Bay support a more southerly or southeasterly source for the Site 1166 mudstones (Supplemental Figure 2).

Nd isotopic ratios (εNd) from van de Flierdt *et al.*, (2008) show large negative εNd values for Unit II, with calculated crustal residence ages of 2.0-3.0 Ga suggesting a very old Proterozoic/Archean upper crustal source material. The ages increase from the bottom of Unit II upward, with the oldest ages coinciding with the peak of mafic enrichment (Figure 2). The εNd crustal residence ages from the Grove Mountains show the majority of rocks ranging from 1.76 to 1.65 Ga, with the exception of felsic orthogneisses that range from 2.46 to 2.27 Ga, and a 50 m wide paragneiss outcrop that contains spinel and has a εNd value of -24.5, with a residence age of 2.99 Ga (Liu *et al.*, 2007). The Southern Prince Charles Mountains region shows εNd values that range from -0.5 to -23 with residence ages from 1.66 to 3.85 Ga (Mikhalsky *et al.*, 2013). Based on the εNd values, crustal residence ages, and the REE enrichment, it is likely that either the Gamburtsev Subglacial Mountains or the Grove Mountains were the source material for the mafic component in the interglacial mudstones. Veevers *et al.* (2008) favored a Gamburtsev Subglacial Mountains source for the Eocene sands underlying the interglacial mudstone section at Site 1166.

The Gamburtsev Subglacial Mountains are considered to be the nucleation point for ice growth in the Prydz Bay region (DeConto & Pollard., 2003). Late Eocene drainage and topographic reconstructions (van de Flierdt *et al.*, 2008; Wilson *et al.*, 2012) indicate that a glacial path from this nucleation point would travel through the

Southern Prince Charles Mountains and the Lambert Graben, eventually draining into Prydz Bay (Figure 1). It has been established that Site 1166 during the late Eocene was ice proximal (Strand *et al.*, 2003), meaning that a glacier was present in the hinterland of Prydz Bay. One explanation as to why the mafic component is not seen earlier (Figure 2) may lie in glacial retreat to the southern portion of the Lambert Graben (Thomson *et al.*, 2013). Sedimentary facies and increasing CIA suggest that the outlet glaciers were retreating from the sediment filled ancient rift valleys onto higher cratonic terranes.

Site U1360

High Al_2O_3/TiO_2 ratios >35 appear in sandy diamict and sandy mudstone samples in Core 6R at the base of the early Oligocene glacial sediments in Site U1360 (Figures 3, 4). Whereas grain-size does not appear to be correlative to the detrital sediment ratios, pre-glacial weathering could be responsible for the high Al_2O_3/TiO_2 ratios. Young & Nesbitt (1998) discuss a similar data sequence and attribute the elevated Al_2O_3/TiO_2 ratios at the base of the Proterozoic Gowganda glacial sequence to the incorporation of weathered material from the pre-glacial substrate at the onset of glaciation. This interpretation is supported by the presence of abundant marine palynomorphs *Vozzhennikovia* spp. and *Enneadocysta diktyostila* of the Transantarctic Flora, and *Nothofagus* and saccate pollen in the same core (Houben *et al.*, 2013). Similarly, Zr/Sc, Zr/Sm and U/Th ratios in Core 6R are likely affected by the incorporation of pre-glacial weathered material into the basal glacial sediment. Besides these samples from Core 6R in Site U1360, the elemental ratios of the overlying sediments consistently point to a more felsic terrain. This is consistent with the REE and other trace elemental depletions (Figure 7). However, the Al_2O_3/TiO_2 ratios of 27-30 for the mudstones in Core 4R that was not affected by pre-glacial sediment recycling are higher than the values of 20-22 found for Plio-Pleistocene diamictites in Core 1R at Site U1360 (Shipboard Scientific Party, 2011) and at nearby Site U1358 (Orejola *et al.*, 2014). Muscovite-biotite and biotite granite clasts were found in dredges off the coast (Goodge & Fanning, 2010), and were interpreted to be sourced from the Mertz Glacier. Our data suggests that during the early Oligocene the dominant sediment source to Site U1360 came from these granites to the East of the Mertz Glacier region (Goodge & Fanning, 2010). This is consistent with reconstructions of crustal thickness and erosion modeling that suggest most of the glacial erosion since ice inception took place to the northwest within the

Wilkes Subglacial Basin, directly inland from Site U1360 in an area overlapping with the western and central basins (Jordan *et al.*, 2013). After pre-glacial sediment was evacuated, incision into granitic basement rocks is evident from the composition of the early Oligocene glaciomarine mudstones at Site U1360. These mudstones have detrital geochemical compositions very similar to the PAAS (Figure 6), except for enrichments in Y, higher Al/Ti oxide and Th/U ratios, lower Zr/Hf ratios and depletion in LREE (Figure 7). The geochemical signature of these U1360 mudstones could be derived from younger evolved granitic intrusions that are hypothesized to be hosted within the cratonic complex of metamorphosed Precambrian - Ordovician igneous and sedimentary basement (Fitzsimons, 2000; Aitken *et al.*, 2014).

Paleoclimatic conditions

The paleoclimate of the glacial foreland is strongly coupled to the advance and retreat of an ice sheet. At Site 1166 in Prydz Bay diatom productivity in the late Eocene was good with neritic to open marine diatom assemblages in Unit II indicating water depths >50m (Shipboard Scientific Party, 2001). Diatom assemblages with high abundance of planktonic species suggest open marine conditions for the interval of ~142-147 mbsf with high biogenic opal content. The presence of iron sulfide below ~140 mbsf (Florindo *et al.*, 2003) may point to suboxic bottom conditions, which could also explain the lack of bioturbation and the well-preserved lamination at the bottom of this mudstone interval (Figure 2). These observations are consistent with a stratified water column, which can be explained by an influx of meltwater from a smaller ice sheet or ice cap grounded on land.

Indeed, the calculated CIA values for late Eocene sediments of Unit II in Prydz Bay indicate a dominant chemical weathering regime, with values exceeding 65. The Eocene values are consistent with previous studies from the area that range from ~67 to 80 (Passchier *et al.*, 2013, 2017). Lower values of 68 may indicate an increase in physical weathering (Passchier *et al.*, 2017), but does not likely indicate continental-scale ice sheet growth. Higher values of 77-80 indicate a more intense chemical weathering period, consistent with higher temperatures and increased precipitation with an absence of physical weathering. Contrastingly, the Neogene diamict that unconformibly overlies these sediments indicates a dominant physical weathering regime, with a value of 57, which is in the same range as Pleistocene diamictons in Prydz Bay (Passchier *et al.*, 2017).

MAT values calculated from the S-index, range from ~10 to ~14˚C for the late Eocene and provide an average for the source region of the detrital sediment. For the coast of Prydz Bay, Tibbett *et al.* (2021) found using the Methylation of Branched Tetraether (MBT) proxy that average mean annual air temperatures (MAAT) were ~14˚C with a maximum of 20˚C. MAP values based on the CIA-K ratio for the Prydz Bay region during the late Eocene range from ~906 mm to ~1171 mm. These values are consistent with a warm and humid environment, in agreement with the dominant kaolinite clay mineralogy found at the base of Unit II at Prydz Bay (O'Brien *et al.*, 2001). Macphail & Truswell (2004) described a low diversity of angiosperm species of *Nothofagus*, Araucariaceae and Podocarpaceae in the upper Eocene sediments of Site 1166, interpreted as a cool-cold temperate rainforest scrub environment. It is mentioned that similar modern-day taxa are found in regions with 1200-2500 mm/yr precipitation (Macphail & Truswell, 2004). Whereas the detrital sediment MAP is an average for the entire catchment from which the sediment was derived, the vegetation was likely concentrated along the coast.

Carter *et al.* (2017) suggest based on apatite fission track and zircon U-Pb ages of ice rafted debris (IRD) found at distal Site 696, that widespread glaciation would have been present by ~36 Ma, enough so that glacial ice would have reached the ocean in the southern Weddell Sea sector. On the other side of East Antarctica, based on the presence of tunnel valleys, Gulick *et al.* (2017) argued that a dynamic marine terminating ice sheet was present in the Aurora Basin from the Eocene to the Miocene. However, this contrasts with the persistent low erosion rates determined for the East Antarctic source areas of sediments of similar age in Prydz Bay (Cox *et al.*, 2010). Furthermore, Galeotti *et al.* (2016) using sediment cores from the Ross Sea, suggested that a full-scale ice sheet was not present until ~32 Ma.

The combined CIA, temperatures, and precipitation from this study on Site 1166 in Prydz Bay do not suggest a significant glacial rock flour contribution from East Antarctica during the ~35.7 Ma interglacial (Nesbitt and Young, 1982, Passchier *et al.*, 2013), meaning, it is likely that during part of the late Eocene, the ice sheet extent was limited and surface conditions were warm and humid (Passchier *et al.*, 2017; Tibbett *et al.*, 2021). This interpretation was confirmed by recent modeling studies that show that even with a maximum topography (Wilson *et al.*, 2012; Paxman, *et al.*, 2019) the late Eocene ice sheet could have had a significantly reduced size in interglacials with a ~100kyr periodicity before the Oi-1 event (Van Breedam *et al.*, 2022).

Contrastingly, early Oligocene sediments from Site U1360 on the Wilkes Land margin show a dominant physical weathering regime, as CIA values for samples, even those that were carbonate corrected, are below 65. This suggests an environment with a larger contribution of glacial rock flour. Temperatures between ~8 and ~10˚C and annual precipitation ranging between ~631 mm and ~731 mm, suggest that the earliest Oligocene interglacial at the Wilkes Land had a cooler and more arid surface climate. The paleoclimate data recovered from the Wilkes Land site, indicates a significant amount of glacial rock flour present at the beginning of the Oligocene (~34 Ma), which is consistent with clay mineralogy showing dominant illite and chlorite and with the abrupt aridification and persistent cooling in East Antarctica reconstructed from other nearby drillsites (Pross *et al.*, 2012; Houben *et al.*, 2013; Passchier *et al.*, 2013).

Conclusions

During the late Eocene interglacial around 35.7 Ma, significant ice was not present in Prydz Bay based on CIA values > 65 (dominant chemical weathering regime) and temperatures in the catchment reaching ~14˚C. Consistent warming was captured from the mudstones recovered at Site 1166, which coincides with a mafic trace element geochemistry with REE enrichment over PAAS. The mudstone section documents a late Eocene glacial retreat cycle with an increase in chemical weathering affecting sediment delivery from ultramafic source areas through time.

Contrastingly, early Oligocene Site U1360 showed CIA values <65 and cooler temperatures indicating a dominantly physical weathering regime, and cold, arid terrestrial environments during deglaciation. High Al_2O_3/TiO_2 ratios at the base of the glacial sequence are likely the result of incorporation of pre-glacial weathered material. Overall, the geochemical study allowed for a better understanding of glacial dynamics in East Antarctica during the late Eocene, as well as the change from Eocene warm humid "greenhouse" interglacials to Oligocene cold and arid "icehouse" deglacial conditions, consistent with the growth of a continental ice sheet in East Antarctica.

Acknowledgements

This research was supported by U.S. National Science Foundation award # ANT 1743643, EAR 1531719, and ANT 1245283 to SP. Dr. Xiaona Li is thanked for her assistance in collecting the ICP-MS data at Montclair State University. This manuscript received two anonymous reviews, which helped to improve the clarity of the text.

Author contributions

JL carried out the sample preparation, instrument analysis, initial data analysis and interpretation, and wrote the first draft of the manuscript in the form of a Master Thesis. SP designed the project and conducted the final writing, drafting, and editing of the manuscript prior to submission with input from JL.

References

Aitken, A.R.A., Young, D.A., Ferraccioli, F., Betts, P.G., Greenbaum, J.S., Richter, T.G., Roberts, J.L., Blankenship, D.D. & Siegert, M.J. 2014. The subglacial geology of Wilkes Land, East Antarctica. Geophysical Research Letters, 41, 7, 2390-2400.

Barker, P.F., Kennett, J.P. 1988. Proceedings of the Ocean Drilling Program, Initial Reports, 113. Ocean Drilling Program, College Station, Texas.

Barth, M.G., McDonough, W.F. & Rudnick, R.L. 2000. Tracking the budget of Nb and Ta in the continental crust. Chemical Geology, 165, 3-4, 197-213.

Blott, S.J. & Pye, K. 2001. GRADISTAT: a grain size distribution and statistics package for the analysis of unconsolidated sediments. Earth Surface Processes and Landforms, 26, 11, 1237-1248.

Bonjour, J.L. & Dabard, M.P. 1991. Ti/Nb ratios of clastic terrigenous sediments used as an indicator of provenance. Chemical Geology, 91, 3, 257-267.

Carter, A., Riley, T.R., Hillenbrand, C., & Rittner, M. 2016. Widespread Antarctic Glaciation during the Late Eocene. Earth and Planetary Science Letters, 458, 49-57.

Ciarletta, D., Characterization of Eocene-Oligocene Depocenters in Prydz Bay, East Antarctica: A Lithostratigraphic Correlation of ODP Sites 739,742, and 1166. Montclair: Montclair State University, 2014. Print.

DeConto, R. M., & Pollard, D. 2003. Rapid Cenozoic Glaciation of Antarctica Induced by Declining Atmospheric CO_2. Nature, 421, 245-248.

Expedition 318 Scientists 2010. Wilkes Land Glacial History: Cenozoic East Antarctic Ice Sheet evolution from Wilkes Land margin sediments. IODP Prel. Rept., 318. doi:10.2204/iodp.pr.318.2010

Ferraccioli, F., Armadillo, E., Jordan, T., Bozzo, E. & Corr, H. 2009. Aeromagnetic exploration over the East Antarctic Ice Sheet: a new view of the Wilkes Subglacial Basin. Tectonophysics, 478(1-2), 62-77.

Fitzgerald, P. 2002. Tectonics and landscape evolution of the Antarctic plate since the breakup of Gondwana, with an emphasis on the West Antarctic Rift System and the Transantarctic Mountains. Royal Society of New Zealand Bulletin, 35, 453-469.

Fitzsimons, I. C. W. 2000. A review of tectonic events in the East Antarctic Shield and their implications for Gondwana and earlier supercontinents. Journal of African Earth Sciences 31, 1, 3-23.

Florindo, F., Bohaty, S.M., Erwin, P.S., Richter, C., Roberts, A.P., Whalen, P.A., & Whitehead, J.M. 2003. Magnetobiostratigraphic chronology and palaeoenvironmental history of Cenozoic sequences from ODP Sites 1165 and 1166, Prydz Bay, Antarctica. Palaeogeography, Palaeoclimatology, Palaeoecology, 198, 69-100.

Galeotti, S., DeConto, R., Naish, T., Stocchi, P., Florindo, F., Pagani, M., Barrett, P.,Bohaty, S.M., Lanci, L., Pollard, D., Sandroni, S., Talarico, F.M., & Zachos, J.C. 2016. Antarctic Ice Sheet variability across the Eocene-Oligocene boundary climate transition. Science, 352(6281), 76-80.

Gasson, E., Lunt, D.J., DeConto, R., Goldner, A., Heinemann, M., Huber, M., LeGrande, A.N., Pollard, D., Sagoo, N., Siddall, M. & Winguth, A. 2014. Uncertainties in the modelled CO 2 threshold for Antarctic glaciation. Climate of the Past, 10, 2, 451-466.

Goldner, A., Herold, N. & Huber, M. 2014. Antarctic glaciation caused ocean circulation changes at the Eocene–Oligocene transition. Nature, 511, 7511, 574-577.

Goodge, J. W., & Fanning, C.M. 2010. Composition and age of the East Antarctic Shield in eastern Wilkes Land determined by proxy from Oligocene-Pleistocene glaciomarine sediment and Beacon Supergroup sandstones, Antarctica. Geological Society of America Bulletin 122, 7-8, 1135-1159.

Gulick, S.P., Shevenell, A.E., Montelli, A., Fernandez, R., Smith, C., Warny, S., Bohaty, S.M., Sjunneskog, C., Leventer, A., Frederick, B. & Blankenship, D.D. 2017. Initiation and long-term instability of the East Antarctic Ice Sheet. Nature, 552(7684), 225-229.

Houben, A.J., Bijl, P.K., Pross, J., Bohaty, S.M., Passchier, S., Stickley, C.E., Rohl, U., Sugisaki, S., Tauxe, L., van De Flierdt, T., Olney, Sangiorgi, M.F., Sluijs, A., Escutia, C., & Brinkhuis, H. 2013. Reorganization of Southern Ocean Plankton Ecosystem at the Onset of Antarctic Glaciation. Science, 340, 341-344.

Jordan, T.A., Ferraccioli, F., Armadillo, E. & Bozzo, E. 2013. Crustal architecture of the Wilkes Subglacial Basin in East Antarctica, as revealed from airborne gravity data. Tectonophysics, 585, 196-206.

Ladant, J. B., Donnadieu, Y., Lefebvre, V., & Dumas, C. 2014. The respective role of atmospheric carbon dioxide and orbital parameters on ice sheet evolution at the Eocene-Oligocene transition. Paleoceanography 29, 8 , 810-823.

Lisker, F., Brown, R. & Fabel, D. 2003. Denudational and thermal history along a transect across the Lambert Graben, northern Prince Charles Mountains, Antarctica, derived from apatite fission track thermochronology. Tectonics, 22, 5.

Liu, X., Jahn, B.M., Zhao, Y., & Zhao, G. 2007. Geochemistry and geochronology of high-grade rocks from the Grove Mountains, East Antarctica: evidence for an Early Neoproterozoic basement metamorphosed during a single Late Neoproterozoic/Cambrian tectonic cycle. Precambrian Research 158, 1, 93-118.

Macphail, M.K., & Truswell, E.M. Palynology of Site 1166, Prydz Bay, East Antarctica. In Cooper, A.K., O'Brien, P.E., & Richter, C. (Eds.), Proc. ODP, Sci. Results, 188 (2004) (Online). Available from World Wide Web: <http://www-odp.tamu.edu/publications/188_SR/013/013.htm>.

Malkowski, M.A., Sharman, G.R., Johnstone, S.A., Grove, M.J., Kimbrough, D.L. & Graham, S.A. 2019. Dilution and propagation of provenance trends in sand and mud: Geochemistry and detrital zircon geochronology of modern sediment from central California (USA). American Journal of Science, 319(10), 846-902.

McLennan, S. M. 2001. Relationships between the trace element composition of sedimentary rocks and upper continental crust. Geochemistry, Geophysics, Geosystems 2,4.

McLennan, S. M., Hemming, S., McDaniel, D.K., & Hanson, G.N. 1993. Geochemical approaches to sedimentation, provenance, and tectonics. Geological Society of America Special Papers 284, 21-40.

McLennan, S. M., Taylor, S.R.., McCulloch, T., & Maynard, J.B. 1990. Geochemical and Nd/ Sr isotopic composition of deep-sea turbidites: Crustal evolution and plate tectonic associations. Geochimica et Cosmochimica Acta 54, 7, 2015-2050.

Murray, R.W., Miller, D.J., & Kryc, K.A. 2000. Analysis of major and trace elements in rocks, sediments, and interstitial waters by inductively coupled plasma–atomic emission spectrometry (ICP-AES). ODP Tech. Note, 29.

Munksgaard, N. C., Thost, D.E., & Hensen, B.J. 1992. Geochemistry of Proterozoic granulites from northern Prince Charles Mountains, East Antarctica. Antarctic Science 4, 1, 59-69.

Mikhalsky, E. V., Boger, S.D., & Henjes-Kunst, F. 2013. The geochemistry and Sm–Nd isotopic systematics of Precambrian mafic dykes and sills in the southern Prince Charles Mountains, East Antarctica. Journal of Petrology 54,12, 2487-2520.

Nakamura, N. 1974. Determination of REE, Ba, Fe, Mg, Na and K in carbonaceous and ordinary chondrites. Geochimica et Cosmochimica Acta 38, 5, 757-775.

Nesbitt, W., & Young., G.M 1982. Early Proterozoic Climates and Plate Motions Inferred from Major Element Chemistry of Lutites. Nature 299(5885), 715-717.

O'Brien, P.E., Cooper, A.K., Richer, C. 2001. Prydz Bay–Cooperation Sea, Antarctica: glacial history and palaeoceanography. Proceedings of the Ocean Drilling Program, Part A. Vol. 188, College Station, Texas.

Passchier, S. Sedimentology, mineralogy and geochemistry of the Sirius Group and other Cenozoic glacigenic sediments from Antarctica: implications for climate and ice sheet history. Electronic Thesis or Dissertation. Ohio State University, (2000). OhioLINK Electronic Theses and Dissertations Center.

Passchier, S., Ciarletta, D.J., Miriagos, T.E., Bijl, P.K., & Bohaty, S.M. 2017. An Antarctic stratigraphic record of stepwise ice growth through the Eocene-Oligocene transition. Geological Society of America Bulletin 129, 3-4, 318-330.

Passchier, S., Bohaty, S.M., Jiménez-Espejo, F., Pross, J., Röhl, U., Van De Flierdt, T., Escutia, C., & Brinkhuis, H. 2013. Early Eocene to Middle Miocene Cooling and Aridification of East Antarctica. Geochemistry, Geophysics, Geosystems 14, 5, 1399-1410.

Passchier, S., Ciarletta, D.J., Henao, V. & Sekkas, V. 2019. Sedimentary processes and facies on a high-latitude passive continental margin, Wilkes Land, East Antarctica. Geological Society, London, Special Publications, 475(1), 181-201.

Paxman, G.J., Jamieson, S.S., Hochmuth, K., Gohl, K., Bentley, M.J., Leitchenkov, G. & Ferraccioli, F. 2019. Reconstructions of Antarctic topography since the Eocene–Oligocene boundary. Palaeogeography, Palaeoclimatology, Palaeoecology, 535, p.109346.

Peucat, J. J., Capdevila, R., Fanning, C. M., Ménot, R. P., Pécora, L., & Testut, L 2002. 1.60 Ga felsic volcanic blocks in the moraines of the Terre Adélie Craton, Antarctica: comparisons with the Gawler Range Volcanics, South Australia. Australian Journal of Earth Sciences 49, 5, 831-845.

Plank, T. & Langmuir, C.H., 1998, The chemical composition of subducting sediment and its consequences for the crust and mantle. Chemical Geology, 145, 3-4, 325-394.

Pross, J., Contreras, L., Bijl, P.K., Greenwood, D.R., Bohaty, S.M., Schouten, S., Bendle, J.A., Röhl, U. Tauxe,L. Raine, I., Huck, C.E., van de Flierdt, T., Jamieson, S.S.R., Stickley, C.E., van de Schootbrugge, B., Escutia, C., Brinkhuis H., & Integrated Ocean Drilling Program Expedition 318 Scientists 2012. Persistent near-tropical warmth on the Antarctic continent during the early Eocene epoch. Nature 488,7409, 73-77.

Sheldon, N. D., Retallack, G.J., & Tanaka, S. 2002. Geochemical Climofunctions from North American Soils and Application to Paleosols across the Eocene Oligocene Boundary in Oregon. The Journal of Geology 110: 687-96.

Sheraton, J. W., Tindle, A.G., & Tingey, R.J. 1996. Geochemistry, origin, and tectonic setting of the Prince Charles Mountains, Antarctica. AGSO Journal of Australian Geology and Geophysics 16, 345-370.

Stagg, H.M.J. 1985. The structure and origin of Prydz Bay and MacRobertson shelf, East Antarctica. Tectonophysics, 114(1-4), 315-340.

Stocchi, P., Escutia, C., Houben, A.J., Vermeersen, B.L., Bijl, P.K., Brinkhuis, H., DeConto, R.M., Galeotti, S., Passchier, S., Pollard, D. & Klaus, 2013. A Relative sea-level rise around East Antarctica during glaciation. Nature Geoscience 6, 5, 380-384.

Strand, K., Passchier, S., & Näsi, J. 2003. Implications of Quartz Grain Microtextures for OnsetEocene/Oligocene Glaciation in Prydz Bay, ODP Site 1166, Antarctica. Palaeogeography, Palaeoclimatology, Palaeoecology, 198, 101-111.

Taylor, S.R. & McLennan, S.M. 1985. The Continental Crust: Its Composition and Evolution. Blackwell, Oxford, 1-312.

Thomson, S.N., Reiners, P.W., Hemming, S.R., & Gehrels, G.E. 2013. The contribution of glacial erosion to shaping the hidden landscape of East Antarctica. Nature Geoscience 6, 3, 203-207.

Tibbett, E.J., Scher, H.D., Warny, S., Tierney, J.E., Passchier, S. & Feakins, S.J. 2021. Late Eocene record of hydrology and temperature from Prydz Bay, East Antarctica. Paleoceanography and Paleoclimatology, 36(4), p.e2020PA004204.

Van Breedam, J., Huybrechts, P. & Crucifix, M. 2022. Modelling evidence for late Eocene Antarctic glaciations. Earth and Planetary Science Letters, 586, 117532.

van de Flierdt, T., Hemming, S. R., Goldstein, S. L., Gehrels, G. E., & Cox, S. E. 2008. Evidence against a young volcanic origin of the Gamburtsev Subglacial Mountains, Antarctica. Geophysical Research Letters, 35, 21, 1-6. doi:10.1029/2008GL035564

Vandenberghe, N., Hilgen, F.J., & Speijer, R. 2012. The Paleogene Period. *In* The Geologic Time Scale 2012. By Felix M. Gradstein. Amsterdam: Elsevier Science, 855-921.

Veevers, J. J., A. Saeed, & P. E. O'Brien, 2008. Provenance of the Gamburtsev Subglacial Mountains from U–Pb and Hf analysis of detrital zircons in Cretaceous to Quaternary sediments in Prydz Bay and beneath the Amery Ice Shelf. Sedimentary Geology, 211, 12-32.

von Eynatten, H., Tolosana-Delgado, R. & Karius, V. 2012. Sediment generation in modern glacial settings: Grain-size and source-rock control on sediment composition. Sedimentary Geology, 280, 80-92.

Wentworth, C.K. 1922. A scale of grade and class terms for clastic sediments. The Journal of Geology, 30, 5, 377-392.

Westerhold, T., Marwan, N., Drury, A.J., Liebrand, D., Agnini, C., Anagnostou, E., Barnet, J.S., Bohaty, S.M., De Vleeschouwer, D., Florindo, F. & Frederichs, T. 2020. An astronomically dated record of Earth's climate and its predictability over the last 66 million years. Science, 369(6509), 1383-1387.

Wilson, D. S., Jamieson, S. S., Barrett, P. J., Leitchenkov, G., Gohl, K., & Larter, R. D. 2012. Antarctic topography at the Eocene–Oligocene boundary. Palaeogeography, Palaeoclimatology, Palaeoecology, 335, 24-34.

Zachos, J., Pagani, M., Sloan, L., Thomas, E. & Billups, K., 2001. Trends, rhythms, and aberrations in global climate 65 Ma to present. Science, 292(5517), 686-693.

Figure captions

Figure 1. Locations of ODP Site 1166 and IODP Site U1360 on a topographic model for the Eocene of Paxman *et al.*, 2019. Geological interpretations after Goodge and Fanning, 2010; Jordan *et al.*, 2013; Sheraton *et al.*, 1996, Liu *et al.*, 2007.

Figure 2. Lithological log and downcore distribution of particle size and geochemical data for Site 1166 in Prydz Bay. The silt/clay ratio is determined based on laser particle size analysis of the < 2-mm sediment matrix, with the clay-silt boundary at 4 µm. The Al/Ti, Zr/Sm and Cr/V ratios vary with sediment provenance, with Cr/V ratios also affected by chemical weathering (see the main text for details). The CIA refers to the Chemical Index of Alteration. The Mean Annual Precipitation (MAP) values are derived from the CIA-K, and the Mean Annual Temperature (MAT) values are derived from the S-index (Passchier *et al.*, 2013; Sheldon *et al.*, 2002). Lithological log is from Passchier *et al.*, 2017. The magnetostratigraphy is from Florindo *et al.*, 2003. The eNd column refers to the εNd composition of the mud fraction from van de Flierdt *et al.,* 2008.

Figure 3. Lithological log and downcore distribution of particle size and geochemical data for Site U1360 off Adélie Land. The silt/clay ratio is determined based on laser particle size analysis of the < 2-mm sediment matrix, with the clay-silt boundary at 4 µm. The Al/Ti, Zr/Sm and Cr/V ratios vary with sediment provenance, with Cr/V ratios also affected by chemical weathering (see the main text for details). The CIA refers to the Chemical Index of Alteration. The Mean Annual Precipitation (MAP) values are derived from the CIA-K, and the Mean Annual Temperature (MAT) values are derived from the S-index (Passchier *et al.*, 2013; Sheldon *et al.*, 2002). Lithological log is from Passchier *et al.*, 2019. The magnetostratigraphy is from Houben *et al.*, 2013.

Figure 4. Particle size distribution of samples from Sites 1166 and U1360 on a sand-silt-clay ternary plot. The grain-size classes are according to Wentworth (1922) with the clay-silt boundary at 4 µm.

Figure 5. The timing of the late Eocene and early Oligocene deglaciation sequences of Sites 1166 and U1360 relative to the calculated insolation at 70 degrees South (Laskar, 2004). Magnetic polarity chrons according to GTS 2012 (Vandenberghe *et al.*, 2012).

Figure 6. Bivariate plots for the analysis of the detrital geochemistry and provenance of the mudstones from Sites 1166 in Prydz Bay and U1360 off Adélie Land. Star designates the composition of the PAAS (Taylor & McLennan, 1985; Barth et al., 2000). The size of the marker is proportional to the sand % in the <2 mm fraction. A) Al/Ti oxide wt. % vs. Zr/Hf ratios separate felsic from mafic igneous sources and fractionated melt-derived (low Zr/Hf) from primitive melt-derived (high Zr/Hf), such as Ocean Island Basalt (OIB); B) Nb/Ta vs. Zr/Sm ratios showing interglacial mudstone samples resemble intermediate Andesitic Arc (AA) or PAAS composition with only two samples from Site U1360 showing affinities to early continental crust (cf. Foley et al., 2002); C) Zr/Sc vs. Th/Sc plot showing the passive margin signature of the source regions and the relatively small effects of sediment sorting (cf. McLennan et al., 1993 their Figures 3 and 9) and the Th enrichment of the 1166 samples over the U1360 samples as a result of differences in provenance and chemical weathering; D) La/Th vs. Hf (ppm) show the close affinity in provenance of Antarctic interglacial mudstones and PAAS with a slightly more mafic contribution at Site 1166; E) Y/Ni vs. Cr/V plot shows the enrichment in Y for the Adélie Land samples compared to PAAS and the low Cr/V ratios with slight enrichment in Prydz Bay due to chemical weathering (see text for discussion); F) Th (ppm) vs. Th/U plot (cf. McLennan et al., 1993) showing the effect of U depletion due to metamorphism and chemical weathering on the composition of the 1166 mudstones and the low Th attributed to Archean crustal sources for the samples at the base of Site U1360.

Figure 7. Rare Earth Element (REE) enrichments and depletions relative to the PAAS (Taylor & McLennan, 1985; Barth et al., 2000).

Supplemental Figure 1. Maps of elemental ratios in source rocks around Prydz Bay projected onto the median topography at 34 Ma of Paxman et al. (2019); A) Nb/Ta ratios; B) Sm/Zr ratios; C) Cr/V ratios; D) Al/Ti oxide wt. % ratios. Data from Munksgaard et al., 1992; Sheraton et al., 1996; Liu et al., 2007, 2014, 2016; Sanchez et al., 2021.

Supplemental Figure 2. Comparison of Site 1166 and U1360 mudstone compositions to Archean and post-Archean sedimentary rocks using the Europium anomaly and chondrite-normalized Gd_N/Y_N ratios.

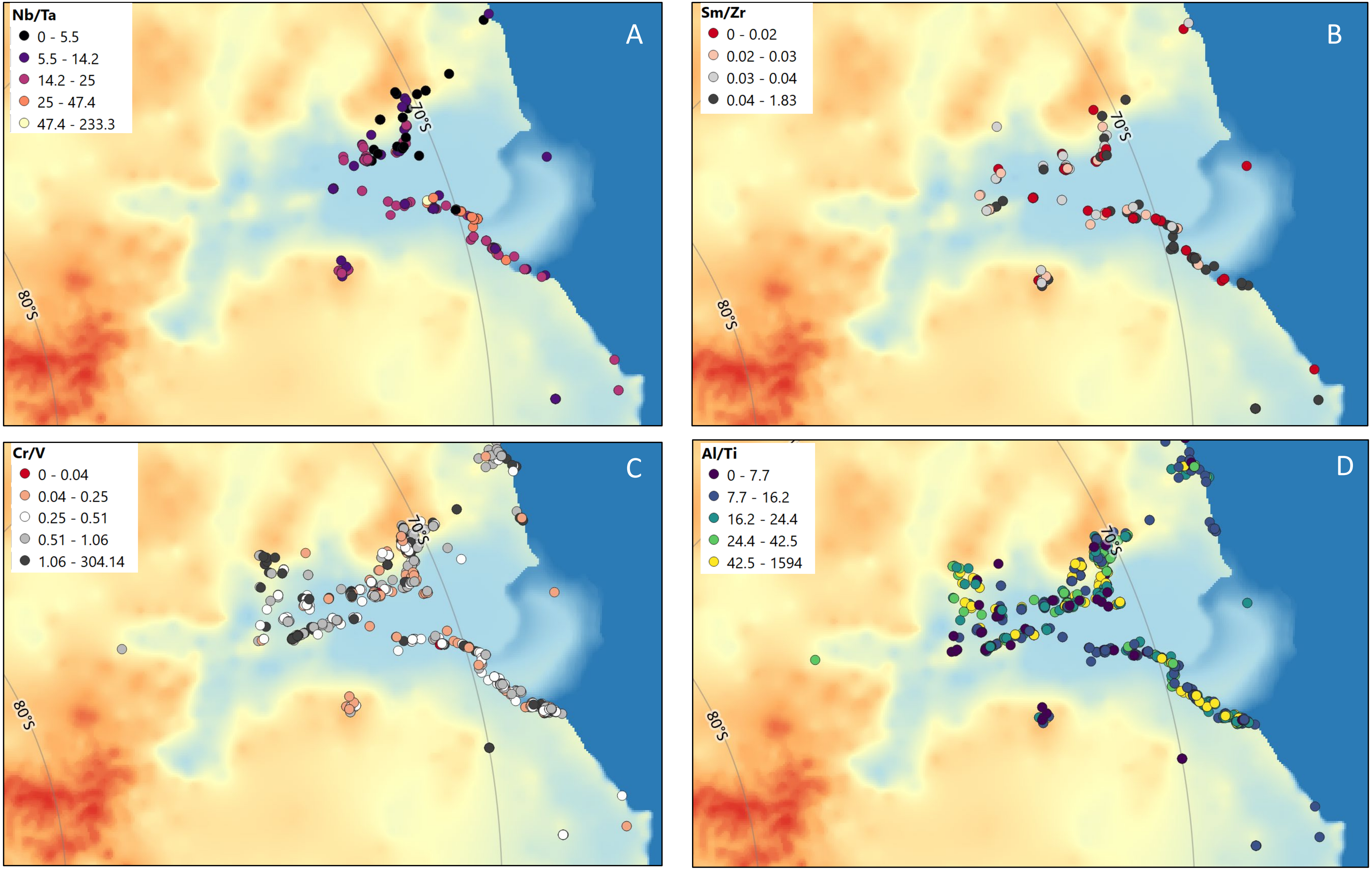
Nb/Ta
0 - 5.5
5.5 - 14.2
14.2 - 25
25 - 47.4
47.4 - 233.3
A
70°S
80°S
Sm/Zr
0 - 0.02
0.02 - 0.03
0.03 - 0.04
0.04 - 1.83
B
70°S
80°S
Cr/V
0 - 0.04
0.04 - 0.25
0.25 - 0.51
0.51 - 1.06
1.06 - 304.14
C
70°S
80°S
Al/Ti
0 - 7.7
7.7 - 16.2
16.2 - 24.4
24.4 - 42.5
42.5 - 1594
D
70°S
80°S

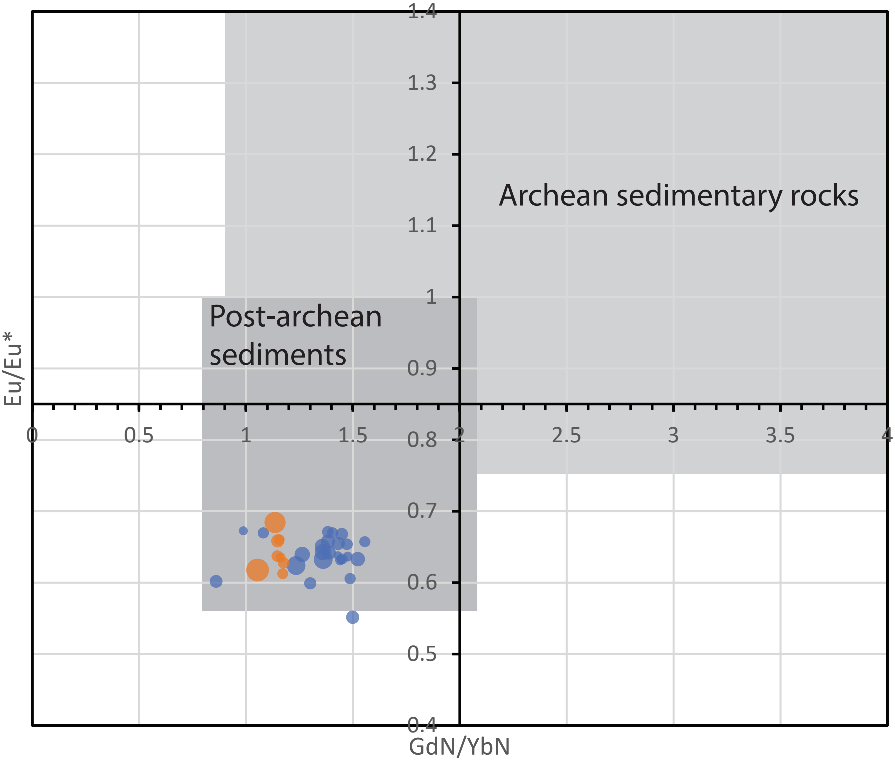
Archean sedimentary rocks
Post-archean sediments
Eu/Eu*
GdN/YbN
1.4
1.3
1.2
1.1
1
0.9
0.8
0.7
0.6
0.5
0.4
0
0.5
1
1.5
2
2.5
3
3.5
4